Optimization of the Synthesis and Physical Characterization of Praseodymium-Doped Type III KGd(PO$_3$)$_4$ Nanocrystals

Irina Adell, Rosa Maria Solé,* Maria Cinta Pujol, Magdalena Aguiló, and Francesc Díaz

Universitat Rovira i Virgili, Departament Química Física i Inorgànica, Física i Cristal·lografia de Materials i Nanomaterials (FiCMA-FiCNA)-EMaS, Campus Sescelades, E-43007 Tarragona, Spain

ABSTRACT: Scintillator materials are used as detectors in the ray imaging techniques for medical diagnosis. Because the ideal medical scintillator material does not exist, many efforts are being made to find new materials that satisfy a greater number of properties. Here, the synthesis conditions of Pr:KGd(PO$_3$)$_4$ nanocrystals by the modified Pechini method are optimized to obtain a single crystalline phase of those that form the polymorphism of KGd(PO$_3$)$_4$. The interest lies in the type III phase because less quenching by Pr^{3+} concentration is expected. By performing transmittance measurements and because of the wide transparency window of the type III KGd(PO$_3$)$_4$ host, the $^3H_4 \rightarrow 5d_1$ absorption transition of Pr^{3+} has been observed in the vacuum ultraviolet spectral range. After creating electron−hole pairs in the host due to the excitation of the material by X-ray radiation, the bands corresponding to the $5d_1 \rightarrow {}^3H_4$, $^3H_5$, $^3H_6$ and $5d_1 \rightarrow {}^3F_3$, $^3F_4$, $^1G_4$ transitions of Pr^{3+} have been observed in the near-visible spectral range, being these 5d → 4f transitions interesting for scintillation applications. Therefore, the type III Pr:KGd(PO$_3$)$_4$ nanocrystals allow the conversion from high-energy radiation to visible or near-visible light.
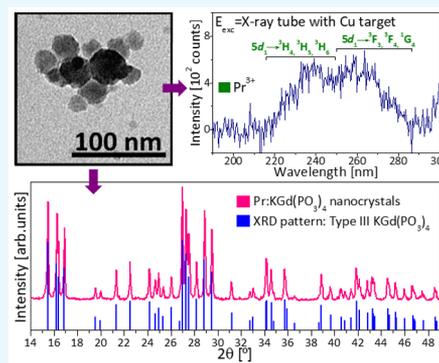
1. INTRODUCTION

Potassium gadolinium phosphate, KGd(PO$_3$)$_4$, hereafter KGdP, is a monoclinic crystal that belongs to the wide family of condensed phosphates of double phosphates of alkali (M) and lanthanide (Ln) ions with the general formula M^{I}Ln^{III}(PO$_3$)$_4$. These condensed phosphates are constituted by corner-sharing PO$_4$ tetrahedra with variable O/P ratio (from 2.5 to 4) building phosphoric anions. Because of the different possibilities of condensation of the phosphoric anions (long chains, rings, and also three-dimensional networks), the condensed phosphates present multiple crystalline structures; so, KGdP can crystallize in three different crystalline structures: type III phase (space group: $P2_1$), type IV (space group: $P2_1/n$), and type B phase (space group: $C2/c$).[1] The first two crystalline structures present long chains of polyphosphates, while the third crystalline structure belongs to the group of cyclophosphates, in which the PO$_4$ forms rings. Besides this structural feature, the coordination of the cations presents differences among these three different crystalline phases.

KGdP can be easily doped with other lanthanide ions, such as praseodymium (Pr^{3+}), because gadolinium (Gd^{3+}) has a high capacity for substitution with lanthanides ions due to the proximity of the ionic radii and the common valence with the other lanthanides ions[1] (ionic radii of Gd^{3+} and Pr^{3+} with coordination VIII are 1.053 and 1.126 Å, respectively[2]). Besides, KPr(PO$_3$)$_4$ and KGdP crystals are isostructural (in the polyphosphate form, with type III phase,[3] and in the cyclophosphate form, with the type B phase[4]). To our

knowledge, there is no evidence of the existence of the KPr(PO$_3$)$_4$ with the type IV crystalline structure.

The transparency window of KGdP extends from 160 nm to 4 μm,[5] which covers the main absorption and emission wavelengths of praseodymium. This UV transparency is a great advantage of this compound to be used as a scintillator material based on the d−f electronic transitions of Pr^{3+} as the doping ion. Scintillator materials are extensively used in technological, industrial, and medical applications.[6] One of its main applications is as a detector in the ray imaging techniques for medical diagnosis.[7−9] In general, an ideal medical scintillator should satisfy the following eight properties to be considered a good scintillator: short decay time, high luminous efficacy, no afterglow, short radiation length, high density, low cost, good spectral match to photodetectors, and high light yield.[10,11] However, until the time, the ideal scintillator does not exist, so each modality of medical imaging systems must select the most suitable combination of properties from the existing scintillators. For this reason, many efforts are being made to find the ideal one. Scintillators can be synthesized in different forms, such as single crystals, powder, thin films, and nanoparticles. Single-crystal sodium iodide doped with thallium ions (NaI (Tl)) is a conventional medical scintillator; however, it does not satisfy with some of the requirements. NaI (Tl) has a comparatively long decay time and a low density.[10] Because the parity allowed f−d transitions in lanthanide ion-

doped materials present high oscillator strengths and the 5d levels have short lifetimes (typically ns), the lanthanide ion-doped materials are an interesting alternative for scintillator materials.[6] García-Murillo et al.[12] proposed europium-doped Gd_2O_3 thin films as a possible good scintillator because of its middle light yield; nevertheless, later this type of films were not considered good as a scintillator for medical imaging because of its comparatively high afterglow. Pedrini et al.[13] studied praseodymium-doped $YAlO_3$, and they found that this material has fast UV fluorescence because of the allowed d−f transitions of Pr^{3+} but relatively low scintillation efficiency. Thus, praseodymium-doped KGdP crystals could be a novel alternative as a scintillator material because the photoluminescence generated by Pr^{3+} ions, after absorbing high-energetic photons by the crystal, in the visible and UV spectral regions through the $5d_1 \rightarrow {}^3H_4$ transition can be observed because of the low UV transparency cut-off of this material.

Moreover, nanocrystalline form allows the possibility to further prepare ceramic materials because of the larger activity in sintering from the nanoscale size[14−16] and also the almost isometric nature of the KGdP structure. In this work, the Pechini method has been used to synthesize KGdP nanocrystals, which previously was successfully used to prepare KNP nanocrystals.[17] This method yields inorganic oxides of excellent phase purity and well-controlled stoichiometry. It also allows obtaining ceramic powders with fine grain size at relatively low temperature through the formation of a polymeric organic net between a metallic acid chelate and a polyhydroxide alcohol by polyesterification. The polymeric network retains homogeneity on the atomic scale and reduces any segregation of the cations. Furthermore, the Pechini method allows to reach various compositions and to vary the nature and the concentration of the doping ion easily.[18−22]

Thus, the first aim of this work is the optimization of the synthesis conditions of type III KGdP nanocrystals doped with praseodymium by the modified Pechini method in order to obtain the nanocrystals in a single crystalline phase. The next goals are to achieve its physical characterization and then its optical spectroscopy to determine whether this material could be a new scintillator material.

2. EXPERIMENTAL SECTION

2.1. Synthesis of the Nanocrystals. A schematic diagram of the modified Pechini synthesis process used for the preparation of Pr:KGdP nanocrystals is shown in Scheme 1, and an illustration of the basic chemical reactions of the Pechini process[19,23] is shown in Scheme 2.

Powders of Pr_6O_{11} (Aldrich Chemical Company Inc., 99.9%), Gd_2O_3 (Aldrich, 99.9%), $NH_4H_2PO_4$ (Fluka Analytical, ≥99.0%), $(NH_4)_2HPO_4$ (Sigma-Aldrich, ≥98%), and K_2CO_3 anhydrous (Alfa Aesar, A Johnson Matthey Company, 99%) were used as starting materials. At first, stoichiometric amounts of Pr_6O_{11} and Gd_2O_3 are converted to the lanthanide nitrate into a quartz crucible by dissolution in concentrated HNO_3 (Merck, 65%) and heated at about 423 K under stirring to evaporate the liquid part. At the same time, stoichiometric amounts of K_2CO_3 and $NH_4H_2PO_4$ or $(NH_4)_2HPO_4$ are dissolved in distilled water into a glass beaker at 323 K.

After that, citric acid, CA, is added as a chelating agent to each container in a specific molar ratio (C_M = [CA]/[METAL]) to prepare metal-chelated CA. C_M describes the degree of the chelation process of the metal in the organic product.[21] To give rise to good reaction between the metal

Scheme 1. Diagram of the Synthesis Process of Pr:KGdP Nanocrystals by the Modified Pechini Method
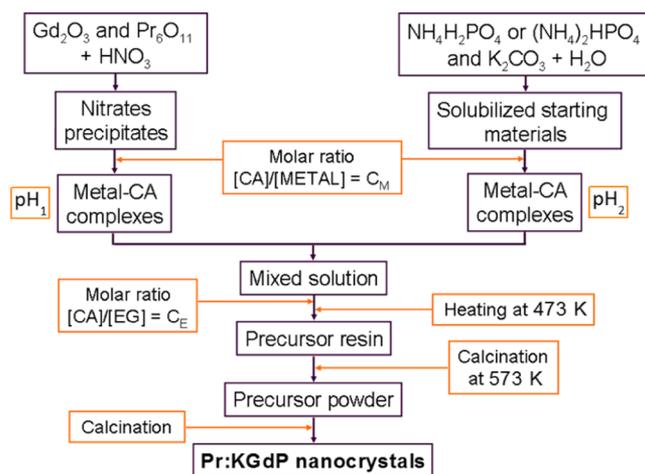
cations and CA, each container is heated at 348 K for 10−20 h under stirring and covered with a crystallizer. On the contrary to other modified Pechini methods used, in this case, we had to use two different containers to avoid the precipitation of gadolinium phosphate.[24] The quartz crucible with gadolinium and praseodymium nitrates is named container 1 and the glass beaker with K_2CO_3 and the phosphate precursor, $NH_4H_2PO_4$ or $(NH_4)_2PO_4$, is named container 2. Just after the incorporation of the CA, the pH in the chelation reaction in container 1 is 1 (pH_1 = 1); it is 2 in container 2 with $NH_4H_2PO_4$ as the phosphate precursor (pH_2 = 2); and the pH in container 2 with $(NH_4)_2PO_4$ as precursor is 3 (pH_2 = 3). Then, in order to study the effect of pH change in the chelation reaction in container 2, the pH_2 was varied by adding NH_4OH just after the incorporation of the CA in Exp. 8, and afterward, the result from this experiment was compared with others.

Then, the content of the two containers are joined in the quartz crucible and they are mixed at 373 K for 4 h under stirring and covered with a crystallizer.

Afterward, ethylene glycol, EG, is added as an esterification agent in a specific molar ratio (C_E = [CA]/[EG]) in order to obtain the polymeric resin. C_E describes the degree of esterification between the hydroxyl groups of EG and the carboxylic acid groups of CA.[21] For this purpose, the reagents are heated at 473 K in a sand bath without being covered and under stirring for 3−4 h. During this step, the viscosity of the product resin gradually increases until the resin gels;[22] at this time, the stirrer is removed. To obtain a drier resin, it is heated at the same temperature of 473 K for a 20 h. This reaction is considered finished when a whitish gel is observed at the bottom of the crucible.

The following step is an initial calcination at 573 K for several hours to start the decomposition of the resin. Thereafter, a product of spongy texture of shiny black color is obtained. To end, this product is grinded in an agate mortar and the resulting precursor powder is calcined at different temperatures in the range from 673 to 1073 K and at air atmosphere for several hours. After each calcination, the resulting powder is grinded in an agate mortar to promote easier removal of the organic parts. These calcinations were performed in a vertical muffle controlled by an Eurotherm temperature controller/programmer.

Scheme 2. Illustration of the Basic Chemical Reactions Involved in the Preparation of the Organic Precursor in the Modified Pechini Method
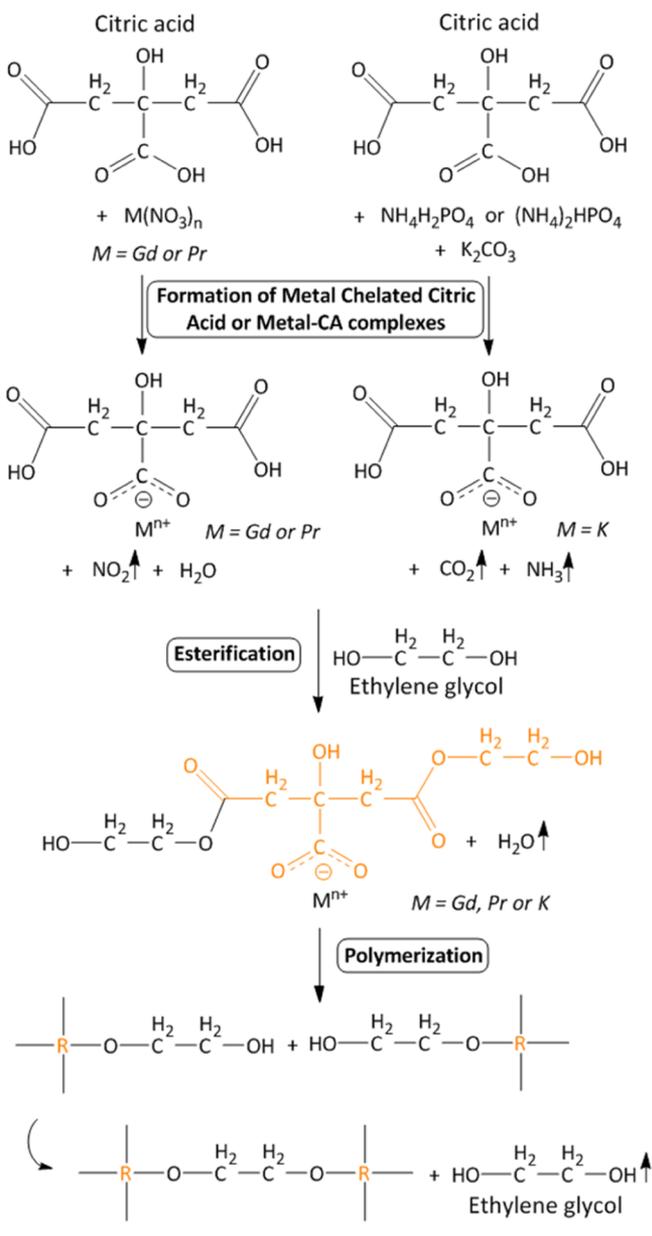
2.2. Characterization Techniques. The crystalline phases of the nanocrystals were identified by X-ray powder diffraction using a Siemens D5000 diffractometer with a Bragg–Brentano parafocusing geometry and vertical θ–θ goniometer, fitted with a curved graphite diffracted-beam monochromator, incident and diffracted-beam Soller slits, a 0.06° receiving slit, and a scintillation counter as a detector. Cu Kα radiation was obtained from a copper X-ray tube operated at 40 kV and 30 mA. For conventional analysis, the X-ray powder diffraction patterns were collected from 5 to 70° of 2θ diffraction range with a step size (ss) of 0.05°, a step time (st) equal to 3 s, and sample rotation. For obtaining diffractograms with lower background noise and thus to be able to identify better the presence of undesirable phases or compounds, the data were collected in a 2θ diffraction range from 10 to 60° with a ss of 0.03°, a st equal to 7 s, and sample rotation. The unit cell

parameters of the non-centrosymmetric phase were calculated using the Rietveld method.[25]

The chemical composition of the nanocrystals was measured quantitatively by electron probe microanalysis (EPMA) using a JEOL JXA-8230 electron microprobe. Before taking the measurements, the samples were prepared in tablet form and one of the two flat faces was sputtered with carbon, which acts as a conductor media to avoid the overcharge of the samples. The electron beam was generated at an intensity of 15 nA and an accelerating voltage of 15 kV. The concentrations of K, P, and O were determined using the Kα X-ray lines of K, P, and O, respectively, and the concentrations of Pr and Gd using the Lα X-ray lines of these elements. The measurement time for Pr was 60 s, while for the other elements was 10 s. In the case of Pr, the measurement time was higher because of its low atomic concentration in the KGdP host.

Differential thermal analysis (DTA) was used to study the thermal evolution of the nanocrystals with the temperature by using a TA Instruments SDT 2960 simultaneous differential scanning calorimetry–thermogravimetric analysis system. The heating rate was at 10 K/min with an air flux of 90 cm^3/min and the Al$_2$O$_3$ was used as a reference.

The morphology, size distribution, and homogeneity of the nanocrystals were observed using a transmission electron microscopy (TEM) JEOL JEM-1011 system with a MegaView III (Soft Imaging System). Previous to the observation of the nanocrystals by TEM, the samples were mixed with ethanol and subsequently were placed in an ultrasound bath for 50 min to reduce and disperse the agglomerates. The TEM images were observed using an accelerating voltage of 80 and 100 kV.

The optical absorption of the praseodymium ion in KGdP nanocrystals was studied by transmittance measurements at room temperature using a Cary 5000 UV–vis–NIR spectrophotometer. The optical absorption spectrum at room temperature of a plate of undoped KGdP single crystal was also obtained in order to help us to label the electronic transitions belonging to praseodymium, using the same apparatus. The undoped KGdP single crystal was grown by the top seeded solution growth—slow cooling technique as reported in Parreu et al.[26]

The emission spectra at room temperature of the Pr:KGdP nanocrystals under 445 nm excitation were obtained using a Cary Eclipse fluorescence spectrophotometer with a xenon lamp as the excitation source. The emission spectra at room temperature under X-ray excitation were performed using an X-ray tube with a copper target operating at 40 kV and 30 mA, available at Servei de Recursos Científics i Tècnics of the Universitat Rovira i Virgili. The X-ray radiation reached the pellet sample with an incident angle of 63° with respect to the pellet sample plane. The luminescence emitted from the sample was collected at 90° with respect to the pellet plane, focused with an UV fused silica biconvex lens, guided with an optical fiber, and detected by an Ocean Optics FLAME-S-UV-VIS-ES spectrometer with a spectral resolution of ~1.5 nm.

3. RESULTS AND DISCUSSION

3.1. Synthesis of KGdP Nanocrystals. Tables 1 and 2 show a summary of the experimental parameters used in the synthesis experiments and the phases obtained. The column entitled as "proportion of phases" refers to the ratio qualitatively estimated between the following two crystalline phases of KGdP: type III (monoclinic, space group: $P2_1$) and type B phase (monoclinic, space group: $C2/c$). The number of

Table 1. Summary of the Experimental Parameters and the Observed Results in the Diffractogram Using $NH_4H_2PO_4$ as a Source of Phosphate Groups[b]

Exp.	C_M	C_E	calcination 1 [K-h]	calcination 2 [K-h]	phase $P2_1$	phase $C2/c$	proportion of phases	presence of other compounds
1	3	2	573-3	1073-3	×			yes
2a	3	2	573-8	973-10	×	×	$P2_1$ ≪< $C2/c$	yes↑
2b				1073-10	×	×	$P2_1$ ≪< $C2/c$	yes↑
3a	3	1	573-10	973-10	×	×	$P2_1$ ≪< $C2/c$	no
3b				1073-10	×	×	$P2_1$ ≪≪ $C2/c$	no
4a[a]	6	2	573-10	773-10	×	×	$P2_1$ ≪≪ $C2/c$	no
4b[a]				873-10	×	×	$P2_1$ ≪≪ $C2/c$	no
4c				973-10	×	×	$P2_1$ ≪≪ $C2/c$	no
4d				1073-10	×	×	$P2_1$ ≪≪< $C2/c$	no
5a[a]	6	1	573-10	773-10	×	×	$P2_1$ ≪< $C2/c$	no
5b[a]				873-10	×	×	$P2_1$ ≪< $C2/c$	no
5c				973-10	×	×	$P2_1$ ≪< $C2/c$	no
5d				1073-10	×	×	$P2_1$ ≪≪ $C2/c$	no
6a[a]	3	2	573-10	773-10	×	×	$P2_1$ ≫≫ $C2/c$	no
6b				873-10	×	×	$P2_1$ ≫≫> $C2/c$	yes
6c				973-10	×	×	$P2_1$ ≫≫> $C2/c$	yes↑
6d				1073-10	×	×	$P2_1$ ≫ $C2/c$	yes↓

[a]Experiment whose diffractogram has a high background noise due to incomplete calcination. [b]In all cases, the atomic percentage of Gd substituted by Pr in KGdP is 1 at. % Pr, the pH in the chelation reaction in the quartz crucible with gadolinium and praseodymium nitrates is 1 ($pH_1 = 1$), and the pH in the glass beaker with K_2CO_3 and $NH_4H_2PO_4$ is 2 ($pH_2 = 2$).

Table 2. Summary of the Experimental Parameters and the Observed Results in the Diffractogram Using $(NH_4)_2HPO_4$ as a Source of Phosphate Groups[d]

Exp.	amount of Pr in KGdP [at. %]	pH_2[a]	calcination 2 [K-h]	calcination 3/4 [K-h]	phase $P2_1$	phase $C2/c$	proportion of phases	presence of other compounds
7a	1	3	773-10		×			yes
7b			673-10	823-10	×	×	$P2_1$ ≫≫> $C2/c$	yes↓
7c			873-10		×			yes
7d			723-10	873-5	×			yes↓
7e			973-10		×			yes↑
7f			1073-10		×	×	$P2_1$ ≫> $C2/c$	yes
8a[b]	1	5[c]	823-10		×	×	$P2_1$ ≫> $C2/c$	yes↑
8b			873-10		×	×	$P2_1$ ≫> $C2/c$	no
8c			723-10	873-5	×	×	$P2_1$ ≫> $C2/c$	yes↓
8d			723-10	873-5/873-10	×	×	$P2_1$ ≫≫> $C2/c$	yes
8e			973-10		×	×	$P2_1$ ≫> $C2/c$	yes↑
8f			1073-10		×	×	$P2_1$ ≫ $C2/c$	yes↑
9a	3	3	723-10	873-5	×	×	$P2_1$ ≫≫> $C2/c$	no
9b			773-10	873-5	×	×	$P2_1$ ≫≫> $C2/c$	no
10	5	3	773-10	873-7	×			no
11	10	3	773-10	873-7	×			no
12	0	3	773-10	873-7	×			no

[a]The pH was measured at the beginning of the chelation reaction in the glass beaker with $(NH_4)_2HPO_4$ and K_2CO_3 reagents. [b]Experiment whose diffractogram has a high background noise due to incomplete calcination. [c]This pH was achieved by adding NH_4OH just after the incorporation of the CA. [d]In all cases, $C_M = 3$, $pH_1 = 1$, $C_E = 2$, and a first calcination at 573 K for 10 h.

> or < symbols is related to the proportion between these two phases. Thus, $P2_1 > C2/c$ means that the intensity of the X-ray diffraction peaks of the $P2_1$ phase is only slightly higher than the corresponding to the $C2/c$ phase, while $P2_1 ≫≫ C2/c$ means that the $P2_1$ is clearly the majority phase and the $C2/c$ is a very minority phase. The column called "presence of other compounds" indicates the presence in the sample of compounds different from the KGdP type III and type B phases. Our interest lies in obtaining solely the type III phase (space group: $P2_1$) because the minor Gd−Gd interatomic distance in this crystalline phase is the longest one in comparison to the other two phases of KGdP (type IV and type B phases), resulting in a priori minor occurrence of the

quenching by Ln^{3+} concentration in the process of emitting light by the optically active lanthanide ions (Ln^{3+}). The minor Gd−Gd interatomic distance is 6.59,[27] 6.316,[28] and 5.269 Å[29] for the type III, type IV and type B phases of KGdP, respectively. Besides, given that the average Gd−O interatomic distance into the Gd coordination polyhedron and its distortion are similar in the three crystalline phases,[27] the Ln^{3+} ions will experience similar interactions with the crystal field.[30] In addition, a distinctive feature of the type III phase is that it is a non-centrosymmetric crystalline phase, which allows it to have nonlinear optical properties. Figure 1 shows a projection of the type III KGdP crystalline structure parallel to the b crystallographic direction, in which the Gd coordination
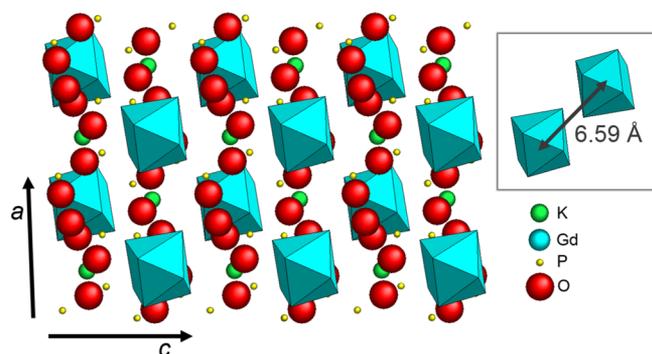
Figure 1. Projection of the type III KGd(PO$_3$)$_4$ structure parallel to the *b* crystallographic direction, showing the Gd coordination polyhedron and the shortest Gd—Gd interatomic distance.

polyhedron and the shortest Gd—Gd interatomic distance can be observed.

The experimental parameters of the first experiment were as follows: an atomic percentage of praseodymium doping ions of 1 at. %, C_M = 3, C_E = 2, a first calcination at 573 K for 3 h, and a second one at 1073 K for 3 h. As it can be observed in Figure 2, the obtained product in Exp. 1 corresponds to a mixture of
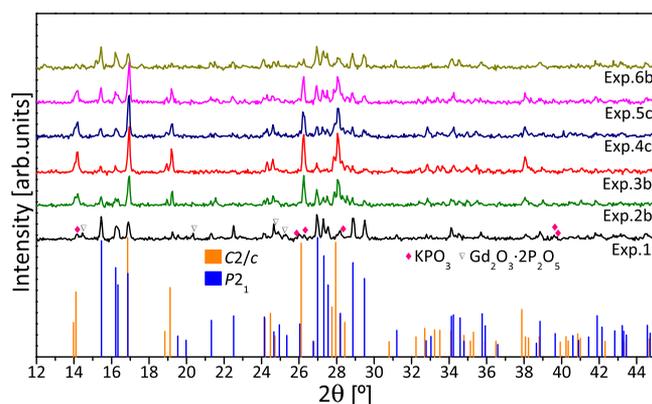
Figure 2. X-ray powder diffractogram pattern for two crystalline phases of KGdP and one experimental diffractogram of Pr:KGdP nanocrystals for each experiment from Exp. 1 to Exp. 6.

Gd$_2$O$_3$·2P$_2$O$_5$ (JCPDS 35-0078), KPO$_3$ (JCPDS 35-0819), which have been identified as intermediate products, and KGdP (*P2$_1$* phase). To provoke the complete synthesis of KGdP as a product and eliminate the presence of other compounds in the final product, the reaction times between the reactants in the chelating, esterification, and polymerization reactions (Scheme 2) under stirring were longer than in Exp. 1 and the time in the two calcinations was also elongated (Exp. 2, 3). The effect of the molar ratios C_M and C_E was also studied (Exp. 3−6). Almost in all these experiments, only KGdP product was obtained and its *C2/c* phase was in a higher proportion than the *P2$_1$* phase, as can be seen in Figure 2. Because there is an overlap of many peaks of the type IV phase pattern with the patterns of the type III and B phases, it is difficult to affirm or discard the presence of a low amount of the type IV phase (monoclinic, space group: *P2$_1$/n*) in these experiments. The ratio of the two majoritarian crystalline phases of KGdP is reverted in Exp. 6 when C_M = 3 and C_E = 2 are used. Thus, C_M = 3 and C_E = 2 seem to be the most suitable molar ratios for obtaining mainly the non-centrosym-

metric crystalline phase of KGdP (space group: *P2$_1$*). From now on, all synthesis experiments were performed using these two molar ratios and a first calcination at 573 K for 10 h.

By comparing Exp. 6, 7, and 8, the effect of the pH change in the chelation reaction can be observed. As explained in the Experimental Section, when NH$_4$H$_2$PO$_4$ was used as the phosphate precursor (Exp. 6), the pH in this reaction was about pH$_2$ = 2. In order to have the reaction in a less acid medium, ammonium phosphate dibasic, (NH$_4$)$_2$HPO$_4$, was used as a source of phosphate groups, leading to an at least pH$_2$ = 3 during this reaction in Exp. 7. Finally, in Exp. 8, ammonium hydroxide, NH$_4$OH, was added just after the incorporation of CA in order to obtain a pH$_2$ = 5. First, it should be noted that the carboxylate ion functions effectively to form metal chelates, whereas the non-ionized carboxylic acid group is not an efficient donor group.[31] The concentration of the carboxylate ion is higher than the one of non-ionized carboxylic acid group when pH > pK_a.[32] Thus, because the logarithmic acid dissociation constant of the first proton of CA is pK_{a1} = 3.13 and of the second one is pK_{a2} = 4.76, CA is found with one carboxylate ion when pH is in the range 3.13−4.75 and with two carboxylate ions when pH is between 4.76 and 6.39.[33] Besides, it should also be noted that the esterification reaction needs to be catalyzed by acid and the non-ionized carboxylic acid group is required in order to have the carbonyl activated toward nucleophilic attack. Thus, a pH$_2$ of at least 3 seems to be the most suitable pH because pH$_2$ = 3.13−4.75 results in a molecule of CA with one carboxylate ion to prepare one metal−CA chelate and with two non-ionized carboxylic acid groups to give rise to the esterification reaction in order to obtain the polymeric organic network. This homogeneous formation of the polymeric network could contribute to obtain a single crystalline phase of KGdP, as it can be observed in Figure 3. Then, the conditions of Exp. 7 are more appropriate to form type III KGdP than the ones for Exp. 6 and 8.

By changing the calcination time, calcination temperature, and number of calcinations, the product obtained presents different ratios of the *P2$_1$* and *C2/c* crystalline phases and different quantity of subproducts. In the Exp. 7, it is observed by these changes in the calcination procedure than a lower temperature in the calcination 2, and the addition of a third
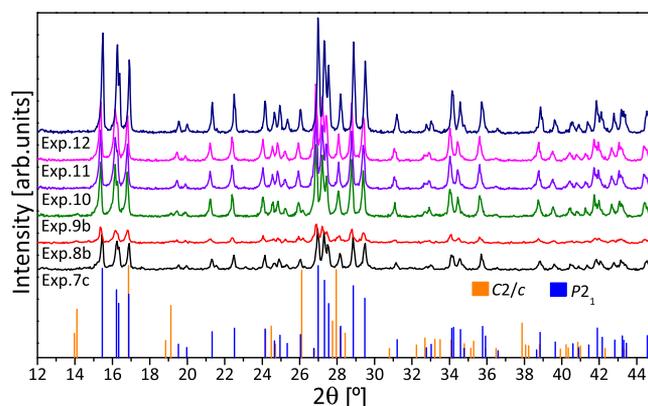
Figure 3. X-ray powder diffractogram pattern for two crystalline phases of KGdP and one experimental diffractogram of Pr:KGdP nanocrystals for each experiment from Exp. 7 to Exp. 12. The diffractograms 9b, 10, 11, and 12 belong to X-ray powder diffraction analysis with ss = 0.03° and st = 7 s.

calcination favors the obtaining of the $P2_1$ crystalline phase and the reduction of the presence of other phases in the final product. In the Exp. 9, 10, 11, and 12, besides change in the concentration of praseodymium of the obtained product, the temperatures and times of calcination 2 and calcination 3 were optimized till obtaining no presence of other compounds and only obtaining the $P2_1$ crystalline KGdP phase in the product. Thus, summarizing, the optimal conditions of calcination are a first calcination at 573 K for 10 h, a second calcination at 773 K for 10 h, and a third calcination at 873 K for 7 h.

Thus summarizing, the optimal parameters to synthesize $KGd_{1-x}Pr_x(PO_3)_4$ nanocrystals with a unique crystalline $P2_1$ phase by the modified Pechini method are $C_M = 1$ with a pH_2 = 3, $C_E = 2$, a reaction time between metal cations and CA of 10−20 h at 348 K under stirring (when the reagents are in two separate containers) followed by 4 h more at 373 K after mixing the content of the containers, a reaction time between metal−CA complexes and EG of around 4 h at 473 K in a sand bath under stirring followed by about 20 h more at the same temperature without stirring, a first calcination at 573 K for 10 h, a second one at 773 K for 10 h, and a third one at 873 K for 7 h.

3.2. Morphological Characterization and Particle Size Distribution.
The morphology, size distribution, and homogeneity of the nanocrystals were observed by TEM. The particle size distribution was estimated using multiple TEM images as the pictures shown in Figure 4. In the same
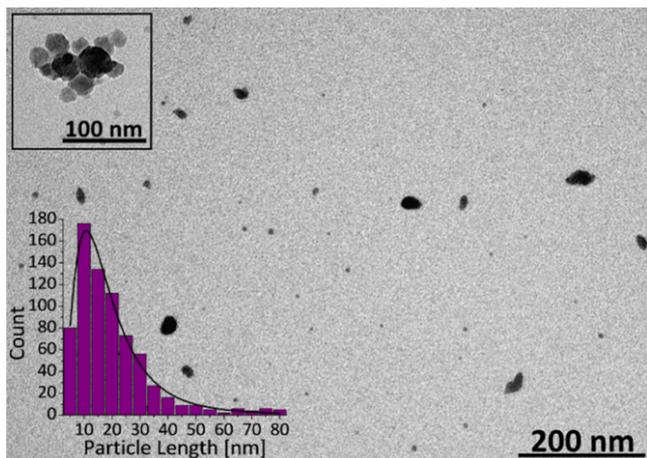
Figure 4. Representative TEM images of 5 at. % Pr:KGdP nanocrystals from Exp. 10 and the total particle size distribution.

figure, the histogram of the particle size distribution of 5 at. % Pr:KGdP nanocrystals is also shown. From the histogram, a predominance of small particles with sizes ranging from 10 to 20 nm can be observed. The distribution of the particle size can be fitted by a lognormal function, as expected in particles prepared by the Pechini method, in which their constitution follows the steps of nucleation, condensation, and crystal particle growth.[34,35]

3.3. Effects of Doping: Changes in Unit Cell Parameters with Praseodymium Doping.
The unit cell parameters and unit cell volume of Pr:KGdP nanocrystals were refined by the Rietveld method.[25] Figure 5 shows the observed, calculated and differential X-ray powder diffraction profile obtained after Rietveld refinement of the 10 at. % Pr:KGdP nanocrystals, as an example. In Table 3, it can be seen how as the praseodymium content increases, the a, b, and c unit cell
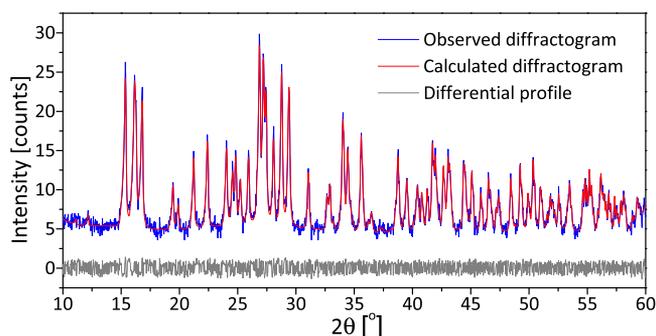
Figure 5. Observed, calculated and differential X-ray powder diffraction profile obtained after Rietveld refinement at room temperature of 10 at. % Pr:KGdP nanocrystals.

parameters and the unit cell volume V increase. However, the increase of the a unit cell parameter is very slight. This increase in the unit cell volume when Pr^{3+} is introduced as the doping ion in the KGdP structure was expected because the ionic radius of Pr^{3+} is higher than that of Gd^{3+} (ionic radii of Gd^{3+} and Pr^{3+} with coordination VIII are 1.053 and 1.126 Å, respectively[2]).

The atomic percentage of praseodymium with respect to gadolinium obtained by EPMA for the sample labeled as 3 at. % Pr:KGdP was 2.8 at. %, for 5 at. % Pr:KGdP was 4.9 at. %, and 8.9 at. % for the sample labeled as 10 at. % Pr:KGdP. The sample labeled as 1 at. % Pr:KGdP was not measured by EPMA because the amount of praseodymium is quite low; however, its atomic percentage with respect to gadolinium is expected to be similar to 1 at. %.

3.4. Thermal Analysis of the Nanocrystals.
Figure 6 shows the DTA thermogram of type III 0, 5, and 10 at. % Pr:KGdP nanocrystals. By DTA of type III KGdP nanocrystals and considering a previous study[26] about how type III KGdP single crystal evolves with temperature between room temperature and 1273 K using DTA and X-ray powder diffraction, it was determined that type III KGdP nanocrystals melt incongruently at 1121 K. The incongruent melting point of type III KGdP single crystal is 1142 K, as reported in ref 26. Because the first ones are nanocrystals, a decrease of its incongruent melting point in relation to the bulk material was already expected, given that a higher surface to volume ratio results in a lower melting temperature.[36,37] From the same Figure 6, it could be observed that as praseodymium content in the nanocrystals increases, the incongruent melting point slightly decreases.

3.5. Optical Spectroscopy of Pr^{3+} in Pr:KGdP Nanocrystals.
Figure 7a shows the transmittance spectra at room temperature of type III 5 at. % Pr:KGdP nanocrystals suspended in distilled water. In order to help us identify the absorption peaks observed in the transmittance spectra, the information obtained from the optical absorption spectrum at room temperature of a plate of undoped KGdP single crystal from 190 to 320 nm (Figure 7b) was used. In Figure 7b, by using the Dieke's diagram,[38,39] all the 4f → 4f electronic transitions of Gd^{3+} at wavelengths higher than 190 nm have been labeled. No other absorption belonging to Gd^{3+} can be observed at longer wavelengths than at 320 nm.

In Figure 7a, a broad and intense band centered at 218 nm and two small peaks centered at 445 and 482 nm can be seen. With regard to the intense broad band, it has been proposed that it belongs to the $^3H_4 \rightarrow 5d_1$ transition of Pr^{3+} because an

Table 3. Unit Cell Parameters and Unit Cell Volume V of Undoped KGdP and Pr-Doped KGdP Nanocrystals

real at. % Pr in KGdP	a [Å]	b [Å]	c [Å]	β [deg]	V [Å³]
0	7.2486(3)	8.3505(3)	7.9204(3)	91.828(3)	479.17(3)
2.8	7.2488(4)	8.3517(4)	7.9215(4)	91.832(3)	479.32(4)
4.9	7.2509(4)	8.3553(5)	7.9247(4)	91.827(4)	479.86(5)
8.9	7.2512(3)	8.3575(4)	7.9285(4)	91.847(4)	480.23(4)
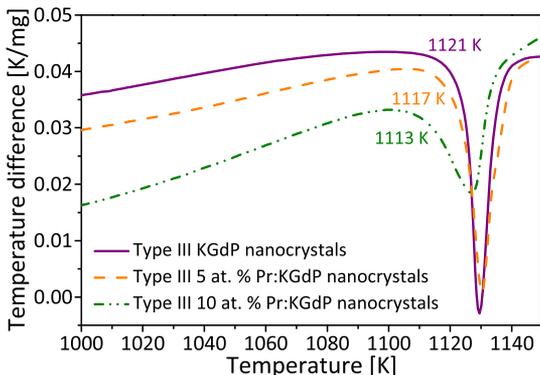
Figure 6. DTA thermogram of type III undoped, 5 and 10 at. % Pr:KGdP nanocrystals.
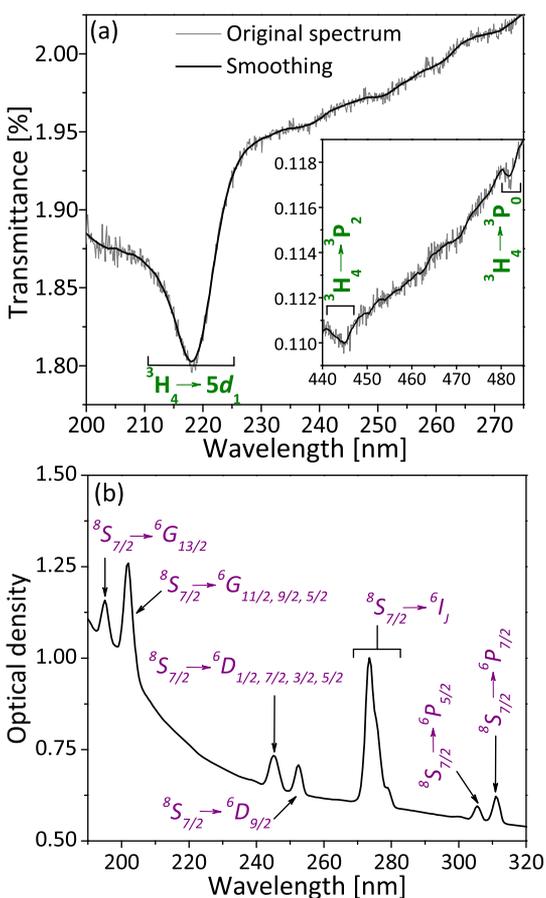
Figure 7. (a) Transmittance spectra of type III 5 at. % Pr:KGdP nanocrystals suspended in distilled water at room temperature. (b) Optical absorption spectrum of a plate of undoped KGdP single crystal at room temperature. In green, the labels corresponding to the electronic transitions of Pr^{3+} assigned to each observed band, and in purple, those corresponding to the electronic transitions of Gd^{3+}.

absorption transition of Gd^{3+} is not expected in this wavelength, as seen in Figure 7b. These 4f → 5d absorption transitions are electric dipole allowed transitions exhibiting very intense and broad bands, and besides, they appear in the spectral range of the vacuum ultraviolet and ultraviolet.[40,41] Thus, the wide transparency window of type III KGdP host allows us to observe the $^3H_4$ → $5d_1$ transition of Pr^{3+}. By using the Dieke's diagram,[38] the peaks which appear at 445 and 482 nm have been labeled as $^3H_4$ → $^3P_2$ and $^3H_4$ → $^3P_0$ electronic transitions of Pr^{3+}, respectively. The 4f → 4f absorption peak centered at 445 nm has the highest intensity of these two absorption transitions because of its quite large electric dipole oscillator strength because of its pseudo-hypersensitive nature.[41]

On the other hand, it is worth commenting that the 4f → 5d absorption transitions of Pr^{4+} in KGdP host are not observed in the spectral range of 180−325 nm. That is, because Pr^{4+} is isoelectronic with Ce^{3+}, similar results can be expected in the case of having the same host doped with Pr^{4+} or Ce^{3+}.[42] Hence, taking into account the work made by Zhong et al.,[43] the 4f → 5d absorption transitions of Ce^{3+} in KGdP host are found at 193, 209, 221, 245, and 307 nm for 4f → $5d_5$, 4f → $5d_4$, 4f → $5d_3$, 4f → $5d_2$, and 4f → $5d_1$ transitions of Ce^{3+}, respectively, so that it can be concluded that the 4f → 5d absorption transitions of Pr^{4+} are not observed in Figure 7. During the calcination process, the polymeric network is decomposed, leading to the formation of carbon oxides in addition to other calcination products, among them Pr:KGdP. The formation of CO as a calcinations product is expected.[44] According to the literature, CO can act as a reducing agent resulting in its oxidation by forming CO_2,[45] and in this case, its oxidation could promote the reduction of praseodymium from Pr^{4+} to Pr^{3+} because Pr^{4+} is a very powerful oxidizing agent.[46,47] Therefore, it is reasonable to assume that praseodymium ions are, in the final product, basically in Pr^{3+} form. Thus, the partial substitution of Gd^{3+} by Pr^{3+} in the crystalline network of KGdP will result in an electrically neutral structure, with higher stability than if Pr^{4+} was present.

Figure 8 shows the emission spectrum at room temperature of type III 5 at. % Pr:KGdP nanocrystals suspended in EG under 445 nm excitation. After exciting them at 445 nm ($^3H_4$ → $^3P_2$ of Pr^{3+}), five emission peaks can be observed in the wavelength range from 590 to 850 nm. Such emission transitions belong to 4f → 4f transitions of Pr^{3+}. By comparing the obtained emission spectrum with the emission spectra of Pr^{3+} doped in $LaAlO_3$,[48] $NaGd(WO_4)_2$,[49] and $La_{1/2}Na_{1/2}TiO_3$[50] hosts as well as Bi^{3+} and Pr^{3+} co-doped lead silicate glasses[51] under Pr^{3+} 4f → 4f excitation and by using the Dieke's diagram,[38] the emission peaks have been labeled as $^1D_2$ → $^3H_4$, $^3P_0$ → $^3H_6$, $^3P_0$ → $^3F_3$, $^3P_0$ → $^3F_4$, and $^1D_2$ → $^3F_2$. Because its photoluminescence under Pr^{3+} 4f → 4f excitation occurs from both $^3P_0$ and $^1D_2$ levels of Pr^{3+}, this means that the emission from the $^3P_0$ level is not quenched because of the presence of an intervalence charge transfer state between these two levels, as happens in perovskite titanates
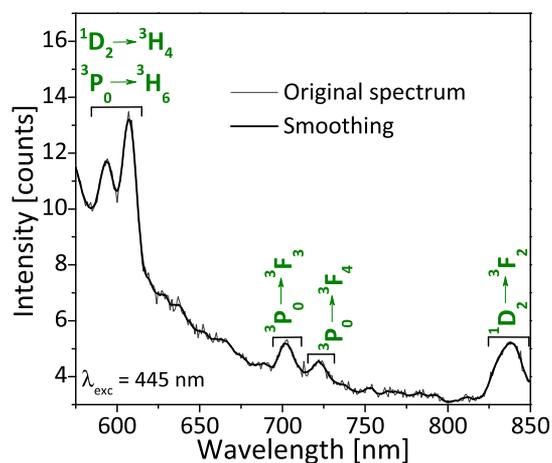
Figure 8. Emission spectrum of type III 5 at. % Pr:KGdP nanocrystals suspended in EG at room temperature under 445 nm excitation ($^3H_4$ → $^3P_2$ of Pr^{3+}). In green, the labels corresponding to the electronic transitions of Pr^{3+} assigned to each observed band.

$R_{1/2}Na_{1/2}TiO_3:Pr^{3+}$ (R = La, Gd, Y, Lu)[50] and in Pr^{3+}- and Tb^{3+}-doped double tungstate crystals $KRE(WO_4)_2$ (RE = Y, Gd, Yb, Lu).[52]

Figure 9 shows the emission spectra at room temperature under X-ray excitation of type III Pr:KGdP nanocrystals
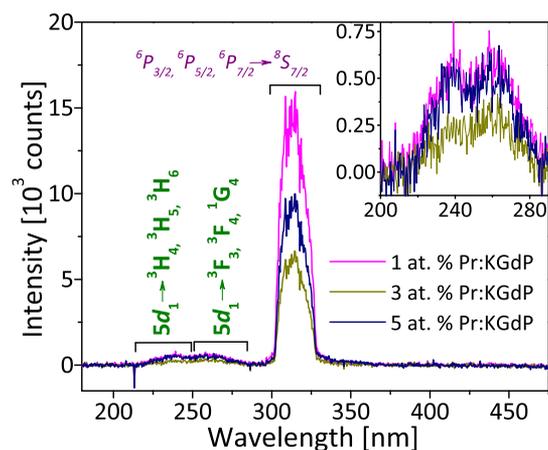
Figure 9. Emission spectra under X-ray excitation of type III 1, 3, and 5 at. % Pr:KGdP nanocrystals as a pellet at room temperature. In purple, the labels corresponding to the electronic transitions of Gd^{3+} assigned to the observed band, and in green, the labels corresponding to the electronic transitions of Pr^{3+} assigned to each observed band.

pressed in a pellet. The most intense band centered at 313 nm corresponds to the $^6P_{3/2}$, $^6P_{5/2}$, $^6P_{7/2}$ → $^8S_{7/2}$ transitions of Gd^{3+}. The low intensity bands centered at around 239 and 261 nm belong to the $5d_1$ → $^3H_4$, $^3H_5$, $^3H_6$ and $5d_1$ → $^3F_3$, $^3F_4$, $^1G_4$ transitions of Pr^{3+}, respectively, and as mentioned earlier, the 5d → 4f transitions of lanthanide ions are of special interest for scintillation applications. The level transition assignation has been done using the Dieke's diagram[38] and taking into account that the energy difference from the $5d_1$ level of Pr^{3+} in type III KGdP host to the $^3H_4$ level is about 45 872 cm^{-1} (5.69 eV, 218 nm). As can be seen in the same figure, there is a different behavior depending on the praseodymium content. Hence, the composition that seems to be the most interesting for scintillation applications is type III KGdP nanocrystals doped

with 5 at. % of Pr because the intensity of the bands corresponding to the $5d_1$ → 4f transitions of Pr^{3+} is the highest and at the same time that the band corresponding to the 4f → 4f transitions of Gd^{3+} is not so intense.

4. CONCLUSIONS

The present paper reports on obtaining type III $Pr:KGd(PO_3)_4$ nanocrystals by the modified Pechini method for first time up to now. As previously stated, the optimal parameters to synthesize $Pr:KGd(PO_3)_4$ nanocrystals with a unique crystalline phase, type III phase (space group: $P2_1$), by the modified Pechini method are $C_M = 3$ with a $pH_2 = 3$, $C_E = 2$, a reaction time between metal cations and CA of 10–20 h at 348 K under stirring followed by 4 h more at 373 K after mixing the content of the two containers, a reaction time between metal–CA complexes and EG of around 4 h at 473 K in a sand bath under stirring followed by about 20 h more at the same temperature without stirring, a first calcination at 573 K for 10 h, a second one at 773 K for 10 h, and a third one at 873 K for 7 h. By using TEM, a predominance of the nanocrystals with sizes ranging from 10 to 20 nm has been observed.

From the transmittance measurements, it has been found that the $^3H_4$ → $5d_1$ transition of Pr^{3+} in type III $Pr:KGd(PO_3)_4$ nanocrystals appears as a broad and intense absorption band centered at 218 nm. In the emission spectra of these nanocrystals under X-ray excitation, several $5d_1$ → 4f transitions of Pr^{3+} and the $^6P_{3/2}$, $^6P_{5/2}$, $^6P_{7/2}$ → $^8S_{7/2}$ transitions of Gd^{3+} have been observed. Therefore, the $5d_1$ level of Pr^{3+} is located within the forbidden band gap of type III $KGd(PO_3)_4$, a fact that was expected due to the wide transparency window of the host.

Despite the lower intensity of the bands corresponding to the $5d_1$ → 4f transitions of Pr^{3+} in comparison with the band corresponding to the 4f → 4f transitions of Gd^{3+}, it would be interesting to excite the nanocrystals under direct f−d excitation to obtain the decay time curves from the $5d_1$ level as well as to excite once again with high-energy radiation to widely study their scintillation properties.

■ AUTHOR INFORMATION

Corresponding Author

*E-mail: rosam.sole@urv.cat. Phone: +34 977558787.

ORCID

Rosa Maria Solé: 0000-0002-5769-4141

Author Contributions

The manuscript was written through contributions of all authors. All authors have given approval to the final version of the manuscript.

Notes

The authors declare no competing financial interest.

■ REFERENCES

(1) Parreu, I. Crystal Growth and Characterization of Ytterbium or Neodymium Doped Type III-KGd(PO$_3$)$_4$. A New Bifunctional Nonlinear and Laser Crystal. Ph.D. Thesis, Rovira i Virgili University, 2006.

(2) Shannon, R. D. Revised Effective Ionic Radii and Systematic Studies of Interatomic Distances in Halides and Chalcogenides. *Acta Crystallogr., Sect. A: Cryst. Phys., Diffr., Theor. Gen. Crystallogr.* **1976**, *32*, 751−767.

(3) Oudahmane, A.; Daoud, M.; Tanouti, B.; Avignant, D.; Zambon, D. KPr(PO3)4. *Acta Crystallogr., Sect. E: Struct. Rep. Online* **2010**, *66*, i59−i60.

(4) Wickleder, M. S. Inorganic Lanthanide Compounds with Complex Anions. *Chem. Rev.* **2002**, *102*, 2011−2088.

(5) Solé, R. M.; Pujol, M. C.; Massons, J.; Aguiló, M.; Díaz, F.; Brenier, A. Growth, anisotropic spectroscopy and laser operation of the monoclinic Nd:KGd(PO3)4crystal. *J. Phys. D: Appl. Phys.* **2015**, *48*, 495502.

(6) Nedelec, J. M. Sol-Gel Processing of Nanostructured Inorganic Scintillating Materials. *J. Nanomater.* **2007**, *2007*, 1−8.

(7) Moses, W. W. Scintillator Requirements for Medical Imaging. Presented at the *5th International Conference on Inorganic Scintillators and Their Applications (SCINT99)*, Moscow, Russian Federation, Aug 16−20, 1999; LBNL-4580.

(8) Conti, M. State of the Art and Challenges of Time-of-flight PET. *Phys. Med.* **2009**, *25*, 1−11.

(9) Cherry, S. R. The 2006 Henry N. Wagner Lecture: Of Mice and Men (and Positrons)—Advances in PET Imaging Technology. *J. Nucl. Med.* **2006**, *47*, 1735−1745.

(10) Liu, B.; Shi, C. Development of Medical Scintillator. *Chin. Sci. Bull.* **2002**, *47*, 1057−1063.

(11) Ogiegło, J. M.; Zych, A.; Jüstel, T.; Meijerink, A.; Ronda, C. R. Luminescence and Energy Transfer in Lu$_3$Al$_5$O$_{12}$ Scintillators Co-doped with Ce^{3+} and Pr^{3+}. *Opt. Mater.* **2013**, *35*, 322−331.

(12) García-Murillo, A.; Le Luyer, C.; Garapon, C.; Dujardin, C.; Bernstein, E.; Pedrini, C.; Mugnier, J. Optical Properties of Europium-Doped Gd$_2$O$_3$ Waveguiding Thin Films Prepared by the Sol-Gel Method. *Opt. Mater.* **2002**, *19*, 161−168.

(13) Pedrini, C.; Bouttet, D.; Dujardin, C.; Moine, B.; Dafinei, I.; Lecoq, P.; Koselja, M.; Blazek, K. Fast Fluorescence and Scintillation of Pr-Doped Yttrium Aluminum Perovskite. *Opt. Mater.* **1994**, *3*, 81−88.

(14) Podhorodecki, A.; Gluchowski, P.; Zatryb, G.; Syperek, M.; Misiewicz, J.; Lojkowski, W.; Strek, W. Influence of Pressure-Induced Transition from Nanocrystals to Nanoceramic Form on Optical Properties of Ce-Doped Y3Al5O12. *J. Am. Ceram. Soc.* **2011**, *94*, 2135−2140.

(15) Trojan-Piegza, J.; Gierlotka, S.; Zych, E.; Lojkowski, W. Spectroscopic Studies of Nanopowder and Nanoceramics La2H-f2O7:Pr Scintillator. *J. Am. Ceram. Soc.* **2014**, *97*, 1595−1601.

(16) Pankratov, V.; Grigorjeva, L.; Chernov, S.; Chudoba, T.; Lojkowski, W. Luminescence Properties and Energy Transfer Processes in Nanosized Cerium Doped YAG. *IEEE Trans. Nucl. Sci.* **2008**, *55*, 1509−1513.

(17) Tkaczyk, S.; Galceran, M.; Kret, S.; Pujol, M. C.; Aguiló, M.; Díaz, F.; Reshak, A. H.; Kityk, I. V. UV-Excited Piezo-Optical Effects in Oxide Nanocrystals Incorporated into PMMA Matrices. *Acta Mater.* **2008**, *56*, 5677−5684.

(18) Pechini, M. P. Method of Preparing Lead and Alkaline Earth Titanates and Niobates and Coating Method using the Same to Form a Capacitor. U.S. Patent 3,330,697, North Adams, Massachusetts, 1967.

(19) Liu, W.; Forrington, C. C.; Chaput, F.; Dunn, B. Synthesis and Electrochemical Studies of Spinel Phase LiMn[sub 2]O[sub 4] Cathode Materials Prepared by the Pechini Process. *J. Electrochem. Soc.* **1996**, *143*, 879−884.

(20) Pimentel, P. M.; Martinelli, A. E.; de Araújo Melo, D. M.; Pedrosa, A. M. G.; Cunha, J. D.; da Silva Júnior, C. N. Pechini Synthesis and Microstructure of Nickel-Doped Copper Chromites. *Mater. Res.* **2005**, *8*, 221−224.

(21) Galceran, M.; Pujol, M. C.; Aguiló, M.; Díaz, F. Sol-gel modified Pechini method for obtaining nanocrystalline KRE(WO4)2 (RE = Gd and Yb). *J. Sol-Gel Sci. Technol.* **2007**, *42*, 79−88.

(22) Morrissey, A. L. Preparation of High Purity Doped Oxides for Fundamental Studies. Ph.D. Thesis, Colorado School of Mines, 2013.

(23) Kwon, S. W.; Park, S. B.; Seo, G.; Hwang, S. T. Preparation of Lithium Aluminate Via Polymeric Precursor Routes. *J. Nucl. Mater.* **1998**, *257*, 172−179.

(24) Lessing, P. A.; Erickson, A. W. Synthesis and Characterization of Gadolinium Phosphate Neutron Absorber. *J. Eur. Ceram. Soc.* **2003**, *23*, 3049−3057.

(25) Rietveld, H. M. A Profile Refinement Method for Nuclear and Magnetic Structures. *J. Appl. Crystallogr.* **1969**, *2*, 65−71.

(26) Parreu, I.; Solé, R.; Gavaldà, J.; Massons, J.; Díaz, F.; Aguiló, M. Crystal Growth, Structural Characterization, and Linear Thermal Evolution of KGd(PO3)4. *Chem. Mater.* **2005**, *17*, 822−828.

(27) Parreu, I.; Carvajal, J. J.; Solans, X.; Díaz, F.; Aguiló, M. Crystal Structure and Optical Characterization of Pure and Nd-Substituted Type III KGd(PO3)4. *Chem. Mater.* **2006**, *18*, 221−228.

(28) Rekik, W.; Naïli, H.; Mhiri, T. Potassium gadolinium polyphosphate, KGd(PO3)4. *Acta Crystallogr., Sect. C: Struct. Chem.* **2004**, *60*, i50−i52.

(29) Ettis, H.; Naïli, H.; Mhiri, T. Synthesis and Crystal Structure of a New Potassium−Gadolinium Cyclotetraphosphate, KGdP4O12. *Cryst. Growth Des.* **2003**, *3*, 599−602.

(30) Rodnyi, P. A. Gadolinium-Containing Crystals. *Physical Processes in Inorganic Scintillators*; CRC Press LLC: Boca Raton, FL, 1997; pp 162−163.

(31) Lindsay, R. C. Food Additives: Chelating Agents (Sequestrants). In *Food Chemistry*, 3rd ed.; Fennema, O. R., Ed.; Marcel Dekker Inc.: New York, 1996; pp 778−780.

(32) Aguilar Sanjuán, M. Desplazamiento de una Reacción Ácido-Base en Función del pH. *Introducción a los Equilibrios Iónicos*, 2nd ed.; Reverté: Barcelona, Spain, 1999; pp 15−16.

(33) Ionization Constants of Organic Acids in Aqueous Solution. In *CRC Handbook of Chemistry and Physics*, 95th ed.; Haynes, W. M., Ed.; CRC Press Taylor & Francis Group: Boca Raton, FL, 2014; pp 5−98.

(34) Granqvist, C. G.; Buhrman, R. A. Ultrafine Metal Particles. *J. Appl. Phys.* **1976**, *47*, 2200−2219.

(35) Söderlund, J.; Kiss, L. B.; Niklasson, G. A.; Granqvist, C. G. Lognormal Size Distributions in Particle Growth Processes without Coagulation. *Phys. Rev. Lett.* **1998**, *80*, 2386−2388.

(36) Galceran, M.; Pujol, M. C.; Carvajal, J. J.; Tkaczyk, S.; Kityk, I. V.; Díaz, F.; Aguiló, M. Synthesis and characterization of KTiOPO4nanocrystals and their PMMA nanocomposites. *Nanotechnology* **2009**, *20*, 035705.

(37) Bhatt, S.; Kumar, M. Effect of Size and Shape on Melting and Superheating of Free Standing and Embedded Nanoparticles. *J. Phys. Chem. Solids* **2017**, *106*, 112−117.

(38) Dieke, G. H.; Crosswhite, H. M. The Spectra of the Doubly and Triply Ionized Rare Earths. *Appl. Opt.* **1963**, *2*, 675−686.

(39) Wegh, R. T.; Donker, H.; Meijerink, A.; Lamminmäki, R. J.; Hölsä, J. Vacuum-ultraviolet spectroscopy and quantum cutting forGd3+inLiYF4. *Phys. Rev. B: Condens. Matter Mater. Phys.* **1997**, *56*, 13841−13848.

(40) Dorenbos, P. The 5d Level Positions of the Trivalent Lanthanides in Inorganic Compounds. *J. Lumin.* **2000**, *91*, 155−176.

(41) Pujol, M. C. Obtenció i Caracterització de Cristalls Monoclínics de KGd(WO$_4$)$_2$ Substituïts amb Lantànids. Ph.D. Thesis, Rovira i Virgili University, 2000.

(42) Pawlak, D.; Frukacz, Z.; Mierczyk, Z.; Suchocki, A.; Zachara, J. Spectroscopic and crystallographic studies of YAG:Pr4+ single crystals. *J. Alloys Compd.* **1998**, *275−277*, 361−364.

(43) Zhong, J.; Liang, H.; Lin, H.; Han, B.; Su, Q.; Zhang, G. Effects of crystal structure on the luminescence properties and energy transfer

between Gd3+ and Ce3+ ions in MGd(PO3)4:Ce3+ (M = Li, Na, K, Cs). *J. Mater. Chem.* **2007**, *17*, 4679−4684.

(44) Braun, E.; Levin, B. C. Polyesters: A review of the literature on products of combustion and toxicity. *Fire Mater.* **1986**, *10*, 107−123.

(45) Brackmann, R.; Toniolo, F. S.; Schmal, M. Synthesis and Characterization of Fe-Doped CeO2 for Application in the NO Selective Catalytic Reduction by CO. *Top. Catal.* **2016**, *59*, 1772−1786.

(46) Cotton, F. A.; Wilkinson, G. Other Tetravalent Compounds. *Advanced Inorganic Chemistry*, 3rd ed.; John Wiley & Sons: New York, 1972; p 1073.

(47) Kiebach, W.-R.; Chatzichristodoulou, C.; Larsen Werchmeister, R. M.; Hagen, A. Determination of Redox-Active Centers in Praseodymium Doped Ceria by In Situ-XANES Spectroscopy. *Chem. Phys. Lett.* **2012**, *537*, 80−83.

(48) Dudek, M.; Jusza, A.; Anders, K.; Lipińska, L.; Baran, M.; Piramidowicz, R. Luminescent properties of praseodymium doped Y2O3 and LaAlO3 nanocrystallites and polymer composites. *J. Rare Earths* **2011**, *29*, 1123−1129.

(49) Durairajan, A.; Thangaraju, D.; Moorthy Babu, S.; Valente, M. A. Luminescence Characterization of Sol-Gel Derived Pr^{3+} Doped $NaGd(WO_4)_2$ Phosphors for Solid State Lighting Applications. *Mater. Chem. Phys.* **2016**, *179*, 295−303.

(50) Boutinaud, P.; Sarakha, L.; Mahiou, R.; Dorenbos, P.; Inaguma, Y. Intervalence charge transfer in perovskite titanates R1/2Na1/2TiO3:Pr3+ (R=La, Gd, Y, Lu). *J. Lumin.* **2010**, *130*, 1725−1729.

(51) Suresh, B.; Purnachand, N.; Zhydachevskii, Y.; Brik, M. G.; Reddy, M. S.; Suchocki, A.; Piasecki, M.; Veeraiah, N. Influence of Bi3+ ions on the amplification of 1.3μm emission of Pr3+ ions in lead silicate glasses for the applications in second telecom window communications. *J. Lumin.* **2017**, *182*, 312−322.

(52) Boutinaud, P.; Bettinelli, M.; Diaz, F. Intervalence charge transfer in Pr3+- and Tb3+-doped double tungstate crystals KRE(WO4)2 (RE=Y, Gd, Yb, Lu). *Opt. Mater.* **2010**, *32*, 1659−1663.